Research in Astronomy and Astrophysics, 24:085003 (10pp), 2024 August https://doi.org/10.1088/1674-4527/ad58a7

GRB 210323A: Signature of Long-lasting Lifetime of Supra-massive Magnetar as the Central Engine from the Merger of Binary Neutron Star

Yingze Shan[1], Xiaoxuan Liu[1], Xing Yang[1], Haoyu Yuan[2], and Houjun Lü[1]
[1] Guangxi Key Laboratory for Relativistic Astrophysics, School of Physical Science and Technology, Guangxi University, Nanning 530004, China; lhj@gxu.edu.cn
[2] Department of Astronomy, School of Physics, Huazhong University of Science and Technology, Wuhan 430074, China
Received 2024 May 22; accepted 2024 June 1; published 2024 July 22

Abstract

Theoretically, a supra-massive neutron star or magnetar may be formed after the merger of binary neutron stars. GRB 210323A is a short-duration gamma-ray burst (GRB) with a duration of lasting ∼1 s. The light curve of the prompt emission of GRB 210323A shows a signal-peaked structure and a cutoff power-law model can adequately fit the spectra with $E_p = 1826 \pm 747$. More interestingly, it has an extremely long-lasting plateau emission in the X-ray afterglow with a duration of $\sim 10^4$ s, and then follows a rapid decay with a decay slope ∼3.2. This temporal feature is challenging by invoking the external shock mode. In this paper, we suggest that the observed long-lasting X-ray plateau emission is caused by the energy injection of dipole radiation from supra-massive magnetar, and the abrupt decay following the long-lasting X-ray plateau emission is explained by supra-massive magnetar collapsing into a black hole. It is the short GRB (SGRB) with the longest X-ray internal plateau emission powered by a supra-massive neutron star. If this is the case, one can estimate the physical parameters of a supra-massive magnetar, and compare with other SGRBs. We also discuss the possible gravitational-wave emission, which is powered by a supra-massive magnetar and its detectability, and the possible kilonova emission, which is powered by *r*-process and magnetar spin-down to compare with the observed data.

Key words: (stars:) gamma-ray burst: general – (stars:) gamma-ray burst: individual (GRB 210323A) – stars: magnetars

1. Introduction

Gamma-ray bursts (GRBs) are classified into two categories by the durations (T_{90}) in γ-ray, e.g., short GRBs (SGRBs) defined as $T_{90} < 2$ s versus long GRBs (LGRBs) defined as $T_{90} > 2$ s, respectively (Kouveliotou et al. 1993). The LGRB progenitors are believed to originate from the death of massive stars because some nearby LGRBs are associated with supernovae (SNe), while SGRBs are considered to be from coalescence events of compact stars, such as neutron star–black hole (NS–BH, Paczynski 1991) mergers, or mergers of neutron star–neutron star (NS–NS, Paczynski 1986). The first direct evidence of NS–NS merger for SGRB is the detection of GW170817 by Advanced LIGO and Virgo associated with SGRB 170817A and its kilonova emission (Abbott et al. 2017, 2017; Goldstein et al. 2017; Zhang et al. 2018). Based on the different types of progenitors for GRBs, Zhang (2006) proposed to adopt Type I (mergers of compact stars) and Type II (massive stars collapse) as the classification of GRBs.

In a merger with a black hole involved, the remnant must be a black hole (Popham et al. 1999; Lei et al. 2009; Liu et al. 2017). For the NS–NS merger case, the remnant may be a stellar-mass black hole or a rapidly spinning NS (e.g., hyper-massive NS with hundreds of milliseconds, supra-massive NS with hundreds of seconds, or a stable NS; Usov 1992; Dai & Lu 1998, 1998; Zhang & Mészáros 2001; Metzger et al. 2011; Lü et al. 2015; Gao et al. 2016; Chen et al. 2017). The remnant of the NS–NS merger is sensitive to the equation of the state of the NS couple. During the NS–NS merger, the neutron-rich ejecta can synthesize elements which are heavier than iron via the process of rapid neutron-capture, which is called as *r*-process. The electromagnetic transients with thermal radiation in the optical band are predicted to release from the *r*-process, and it is called kilonova (Li & Paczyński 1998; Berger et al. 2013; Yang et al. 2015; Jin et al. 2016; Troja 2023). Moreover, the additional energy may be injected to result in more bright kilonova emission if the millisecond-magnetar resides in the central engine, also called mergernova (Metzger et al. 2010; Yu et al. 2013; Gao et al. 2017; Lü et al. 2017; Yuan et al. 2021).

On the other hand, by assuming that the central engine of a short GRB is a magnetar, the rotational energy can be dissipated via electromagnetic (EM) and gravitational-wave (GW) radiations. The "internal plateaus" of X-ray observed in some of the SGRB afterglows are evidence of a central engine with a supra-massive NS. The segment of steep decay following the plateau emission can be naturally explained as supra-massive NS as the central engine which collapses into a black hole. Lü et al. (2015) performed a systematic analysis of SGRBs observed by Swift/BAT to test the possible supra-massive NS as the central engine and found that the surviving time of supra-massive NS is distributed in hundreds of seconds.

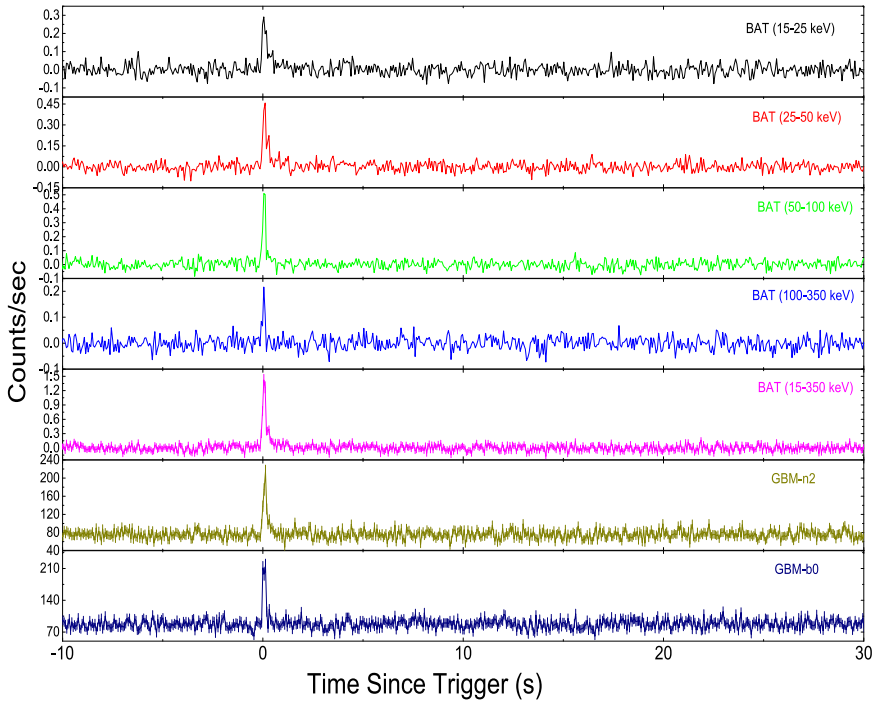

Figure 1. Swift/BAT and Fermi/GBM light curves of GRB 210323A in different energy bands with 64 ms time-bin.

GRB 210323A is a short-hard burst without a redshift measurement. More interestingly, it has an extremely long-lasting plateau emission in the X-ray band with a duration of lasting $\sim 10^4$ s, and then follows a rapid decay. The rapid decay is difficult to interpret by invoking the afterglow model but is consistent with the central engine as a supra-massive magnetar. If this is the case, the surviving time of the supra-massive NS of GRB 210323A is the longest one compared with the other candidates of SGRBs central engine as supra-massive magnetar (Lü et al. 2015). One basic question is whether the properties of the supra-massive magnetar as the central engine for GRB 210323A are different from those of other SGRBs. In this paper, we present our data analysis of GRB 210323A in Section 2. Then, in Section 3, we identify the progenitor of GRB 210323A and compare the properties with those of other GRBs. The details of the physical explanation of data, invoking a supra-massive NS as the central engine of GRB 210323A, possible gravitational-wave (GW) radiation, as well as kilonova emission, are shown in Section 4. The conclusions, along with some discussions, are shown in Section 5.

2. Data Analysis

2.1. Fermi Data Analysis

GRB 210323A was triggered by Fermi/GBM at 22:02:18.40 UT on 2021 March 23 (Hamburg et al. 2021). We adopt the data from the public and official Fermi website,[3] and download the original Time-Tagged-Event data of GRB 210323A. We extract the light curves of GRB 210323A with n2 and b0 detectors for a time-bin of 64 ms (see Figure 1) by adopting the standard heasoft tools from the Fermi official website. The details can be referred to Zhang et al. (2016) and Lan et al. (2018). It is clear to show a single-peaked structure with a $T_{90} \sim 1$ s from 50 to 300 keV.

The time-averaged spectrum of the prompt emission can be extracted after subtracting the background spectra. Here, we selected the time intervals before and after the prompt emission phase as the background in the prompt emission. We adopt the Markov Chain Monte Carlo (MCMC) method to fit the spectra by invoking several models, such as the Band function (Band), power-law (PL) model, cut-off power-law model (CPL), and blackbody (BB). It is found that the best model to describe the observed data is the CPL model by comparing with the goodness of the fits. The CPL model can be described as

$$N(E) = N_0 \cdot E^{\alpha_0} \exp\left(-\frac{E}{E_p}\right), \quad (1)$$

where N_0, E_p, and α_0 are the normalization of the spectrum, peak energy, and photon index, respectively. One has $\alpha_0 = -0.89 \pm 0.07$, and $E_p = 1826 \pm 747$ keV. The spectral fit and the parameter constraints with CPL model are presented in Figure 2.

[3] http://fermi.gsfc.nasa.gov/ssc/data/

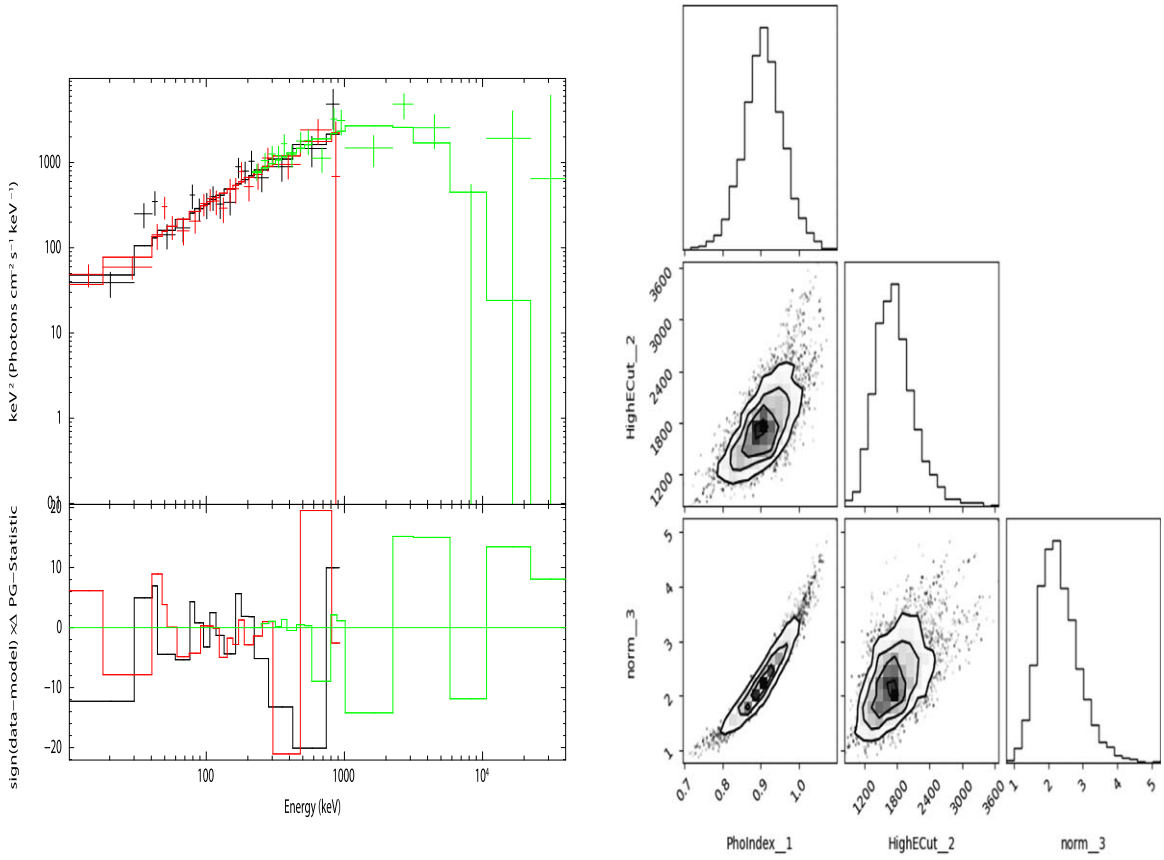

Figure 2. Spectral fits of GRB 210323A with the cut-off power law (CPL) model for Fermi/GBM data. The νF_ν spectrum and parameter constraints of the CPL fit for the burst are shown in the left and right panels, respectively. Histograms and contours in the corner plots show the likelihood map of constrained parameters by using the MCMC. The solid black circles from inside to outside are the 1σ, 2σ, and 3σ uncertainties.

2.2. *Swift Data Analysis*

At 22:02:18 UT on 2021 March 23 (Gropp et al. 2021), GRB 210323A triggered the Swift/BAT. The BAT data were downloaded at the Swift website,[4] and we adopted the standard HEASOFT package to analyze the BAT data. The light curve can be extracted in different energy bands. Similar to the light curve of Fermi/GBM, a single-peaked structure which has a duration $T_{90} \sim 1.12$ s in 15–350 keV is shown in the Swift/BAT light curve (see Figure 1). No evidence of extended emission is found in the BAT energy range up to 30 s after the BAT trigger. A simple power-law model with a spectral index of 1.46 ± 0.17 is the best fitting of the time-averaged spectrum from $T_0 - 0.09$ s to $T_0 + 1.26$ s (Barthelmy et al. 2021).

The Swift X-ray Telescope (XRT) started to observe this source at 88 s after the BAT trigger (Beardmore et al. 2021). We adopt public data from the Swift archive.[5] The X-ray light curve is composed of several segments, such as the initial power-law decay segment with an index $\sim$1.69 before 720 s, and then it becomes flat followed by a steeper segment. Here, we adopted a smoothly broken-power-law (SBPL) function to fit the X-ray data from 750 to 51800 s after the BAT trigger. The SBPL function reads

$$F = F_0 \left[\left(\frac{t}{t_{\rm break}} \right)^{na_1} + \left(\frac{t}{t_{\rm break}} \right)^{na_2} \right]^{-1/n}, \quad (2)$$

where the $t_{\rm break}$ is the break time. a_1 and a_2 are the slope indices before and after the break, respectively. n is the free parameter to describe the breaking sharpness and is fixed to 10 (Liang et al. 2007). One has $a_1 \sim 0.2$, $a_2 \sim 3.25$, and a break time $t_{\rm break} \sim 12{,}000$ s after the BAT trigger. The X-ray light curve and fitting result of GRB 210323A are shown in Figure 3.

The Ultra-Violet Optical Telescope (UVOT; Roming et al. 2005) started to observe the source of GRB 210323A at 89 s after the BAT trigger (Breeveld 2021). However, it does not detect any optical afterglow (Beardmore et al. 2021; Malesani et al. 2021; Pozanenko et al. 2021). Only 3σ upper limits of optical detected are obtained in the early exposures

[4] https://www.swift.ac.uk/burst_analyser/01038247/
[5] https://www.swift.ac.uk/xrt_curves/01038247/

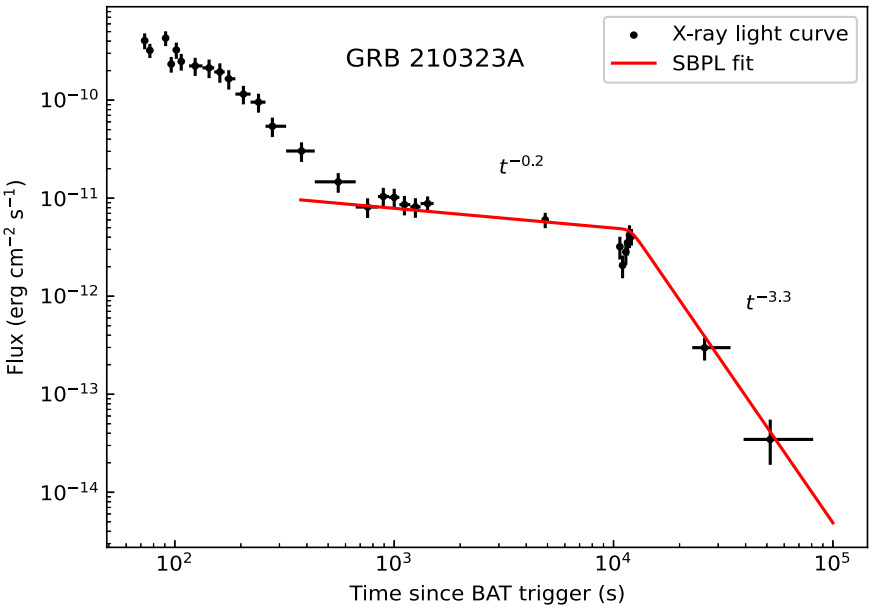

Figure 3. X-ray light curve of GRB 210323A in (0.3–10) keV and the best fit with the smooth broken power law function.

(Breeveld 2021). de Ugarte Postigo et al. (2021) claimed that a low-significance emission line of [O II], which corresponds to redshift $z = 0.37$, but is still not confirmed without finding any evidence for other emission lines.

3. Possible Progenitor of GRB 210323A

From an observational point of view, several lines of evidence suggest that T_{90} may not be a good indicator to reveal the physical origin of GRB (Qin et al. 2013; Kumar & Zhang 2015; Zhang 2018). For example, short-duration GRB 200826A is thought to be produced during the death of massive stars (Ahumada et al. 2021; Zhang et al. 2021), while short-duration with extended emission GRBs 060614, 211227A, 211211A, and 230307A are believed to be produced during mergers of compact stars (Gehrels et al. 2006; Yang et al. 2015; Lü et al. 2022; Troja et al. 2022; Yang et al. 2022; Chang et al. 2023; Ferro et al. 2023; Levan et al. 2023; Sun et al. 2023; Du et al. 2024a, 2024b; Zhong et al. 2024).

In this section, we try to present the $E_{\rm p,z}$–$E_{\gamma,\rm iso}$ correlation (called Amati relation; Amati et al. 2002) for GRB 210323A, and the $\varepsilon \equiv E_{\gamma,\rm iso,52}/E_{\rm p,z,2}^{5/3}$ value defined by Lü et al. (2010) is used to classify the GRBs. Since the redshift of GRB 210323A is unknown, we set a series of pseudo-redshifts of GRB 210323A from 0.01 to 1 to do the calculations. $z = 0.37$ is also taken in this series even it is not confirmed.

3.1. $E_{p,z}$–$E_{\gamma,iso}$ Correlation for GRB 210323A

Amati et al. (2002) discovered a correlation between $E_{\rm p,z}$ and $E_{\gamma,\rm iso}$, e.g., $E_{\rm p}(1+z)$=$E_{\rm p,\,z} \propto E_{\gamma,\rm iso}^{1/2}$ for most long-duration (Type II) GRBs. However, most short-duration GRBs (Type I) are inconsistent with that of long-duration GRBs and seem to be shallower slightly for power index (Zhang et al. 2009). To find out where GRB 210323A is located in the $E_{\rm p,z}$–$E_{\gamma,\rm iso}$ diagram, we calculate $E_{\gamma,\rm iso}$, which is given as:

$$E_{\gamma,\rm iso} = 4\pi k D_{\rm L}^2 S_\gamma/(1+z) = 1.3 \times 10^{50}\ {\rm erg}\ k D_{\rm L,28}^2 S_{\gamma,-7}/(1+z), \quad (3)$$

where $D_{\rm L}$ is the luminosity distance and S_γ is the fluence in observed energy band. Based on the spectral fitting results, one has $S_\gamma = 1.2 \times 10^{-6}\ {\rm erg\ cm^{-2}}$ (Hamburg et al. 2021). In Figure 4, we plot GRB 210323A on the $E_{\rm p,z}$–$E_{\gamma,\rm iso}$ diagram by adopting the pseudo-redshift from $z = 0.01$ to $z = 1.0$. To compare, we also plot other GRBs (e.g., Type I and Type II) in the $E_{\rm p,z}$–$E_{\gamma,\rm iso}$ diagram (Zhang et al. 2009). It is found that GRB 210323A is located far away from the Type II GRBs, but is close to the Type I GRBs when the redshift is larger than 0.1. It suggests that GRB 210323A is likely to be a Type I GRB which is merger-induced.

3.2. ε Value of GRB 210323A

Lü et al. (2010) proposed a novel method for GRB classification (called $\varepsilon-$method) based on $E_{\gamma,\rm iso,52}$ and $E_{\rm p}$. The definition of ε can be given as

$$\varepsilon \equiv E_{\gamma,\rm iso,52}/E_{\rm p,z,2}^{5/3}. \quad (4)$$

We calculate ε value and $T_{90,z} = T_{90}/(1+z)$ of GRB 213223A within redshift range $z = [0.01 \sim 1]$, and overplot it on the $\log\varepsilon - \log T_{90,z}$ diagram (see Figure 5). It is found that GRB

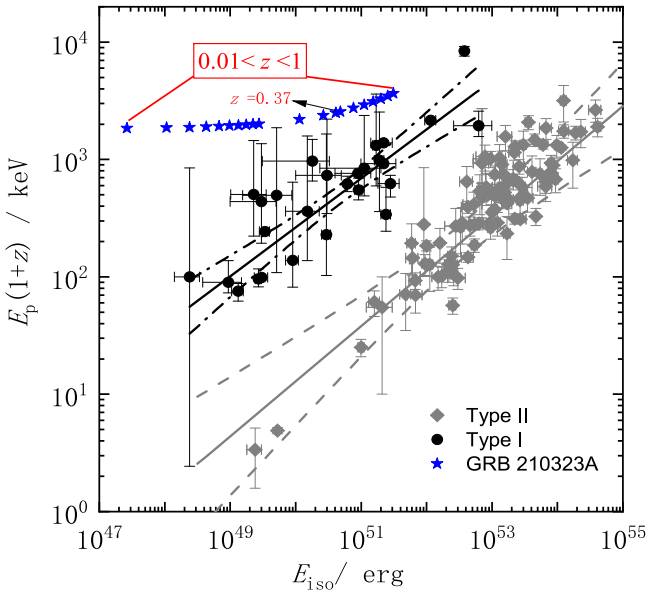

Figure 4. E_p–E_{iso} diagram for Type I, Type II GRBs, as well as GRB 210323A. The black and gray solid lines correspond to best fit with the power-law for the Type I and Type II GRBs, respectively. Dashed borderlines show the 3σ regions for each correlation. The blue stars in the diagram are GRB 210323A with pseudo-redshift in the range of [0.01, 1].

210323A has $\log \varepsilon = -3.72$ with the redshift $z = 0.37$, making it an obvious low-ε GRB population. Even adopting the redshift $z = 0.01 - 1$, the ε value of GRB 210323A remains in the region of the low-ε GRB population. So, it is reasonable to believe that GRB 210323A is a Type I GRB originating from the merger of binary compact stars.

4. The Central Engine, GW Radiation, and Kilonova Emission of GRB 210323A

Following the long-lasting X-ray plateau emission in GRB 210323A afterglow, the sudden decay is difficult to interpret with the external shock model for the BH central engine (Kumar & Zhang 2015; Zhang 2018). However, a highly magnetized fast-spinning neutron star (i.e., a magnetar) can offer a good explanation for the continuous energy injection (Dai & Lu 1998, 1998; Zhang & Mészáros 2001; Troja et al. 2007; Rowlinson et al. 2010; Lü et al. 2015, 2017). The energy injection from the rotation energy lost of magnetar can result in the X-ray plateau emission, and the following abrupt decay segment is the supra-massive magnetar collapsing into a black hole. In this section, we propose using a supra-massive magnetar as the central engine of GRB 210323A to explain the afterglow emission. The observation constraint of possible kilonova emissions and GW radiation is also discussed.

4.1. Supra-massive Magnetar Central Engine

Magnetar serves as an important candidate for powering GRBs. The total energy budget of a magnetar is its rotational energy, which is expressed as

$$E_r = \frac{1}{2} I \Omega^2 \simeq 2 \times 10^{52} \,\mathrm{erg}\, M_{1.4} R_6^2 P_{-3}^{-2}, \quad (5)$$

where M and R are the mass and radius of the NS, respectively. I is the moment of inertia. P and Ω are the period and angular frequency of magnetar, respectively. The rotational energy of magnetar can be lost via magnetic dipole torques (L_E) of spin-down and GW (L_B) radiations. The equation can be expressed as (Zhang & Mészáros 2001; Lasky & Glampedakis 2016)

$$-\frac{dE_r}{dt} = -I\Omega\dot{\Omega} = L_E + L_B = \frac{B_p^2 R^6 \Omega^4}{6c^3} + \frac{32 G I^2 \epsilon^2 \Omega^6}{5c^5}, \quad (6)$$

where B_p is the surface magnetic field, and $\epsilon = 2(I_{xx} - I_{yy})/(I_{xx} + I_{yy})$ is ellipticity of magnetar.

Following the method of Zhang & Mészáros (2001), we suppose that the energy loss is dominated by L_E (ignoring the contribution from GW radiation). The characteristic spin-down luminosity (L_X) and timescale (τ) are written as

$$\tau = \frac{3c^3 I}{B_p^2 R^6 \Omega_0^2} = 2.05 \times 10^3 \mathrm{s}\, I_{45}\, B_{p,15}^{-2}\, P_{0,-3}^2\, R_6^{-6}, \quad (7)$$

$$L_X = \frac{I\Omega_0^2}{2\tau_{c,em}} \simeq 1.0 \times 10^{49} \,\mathrm{erg\ s^{-1}}\, B_{p,15}^2\, P_{0,-3}^{-4}\, R_6^6, \quad (8)$$

where P_0 is the magnetar initial rotating period.

Because of no detection of the spin-down timescale in the X-ray emission of GRB 210323A, one can roughly give the lower limit of the observed break time, i.e.,

$$\tau > t_{col} = t_{break}/(1+z), \quad (9)$$

where t_{col} is collapse time. The X-ray plateau luminosity can be estimated by the luminosity at t_b:

$$L_X \simeq L_b = 4\pi D_L^2 F_{break} \cdot k, \quad (10)$$

where F_{break} is the X-ray flux at t_{break}. Lü et al. (2015) found that the observed luminosity of the X-ray plateau is inverse-proportional to the collapse time. Here, we also plot GRB 210323A in the $L_X - t_{col}$ diagram at the redshift of $z = 0.01$, 0.37, and 1 (in Figure 6). It is found that GRB 210323A seems to be not following the same correlation with that of other SGRBs when the redshift is larger than 1. It suggests that the long-lasting supra-massive magnetar of GRB 210323A is different from that of short-lifetime supra-massive magnetar in other SGRBs.

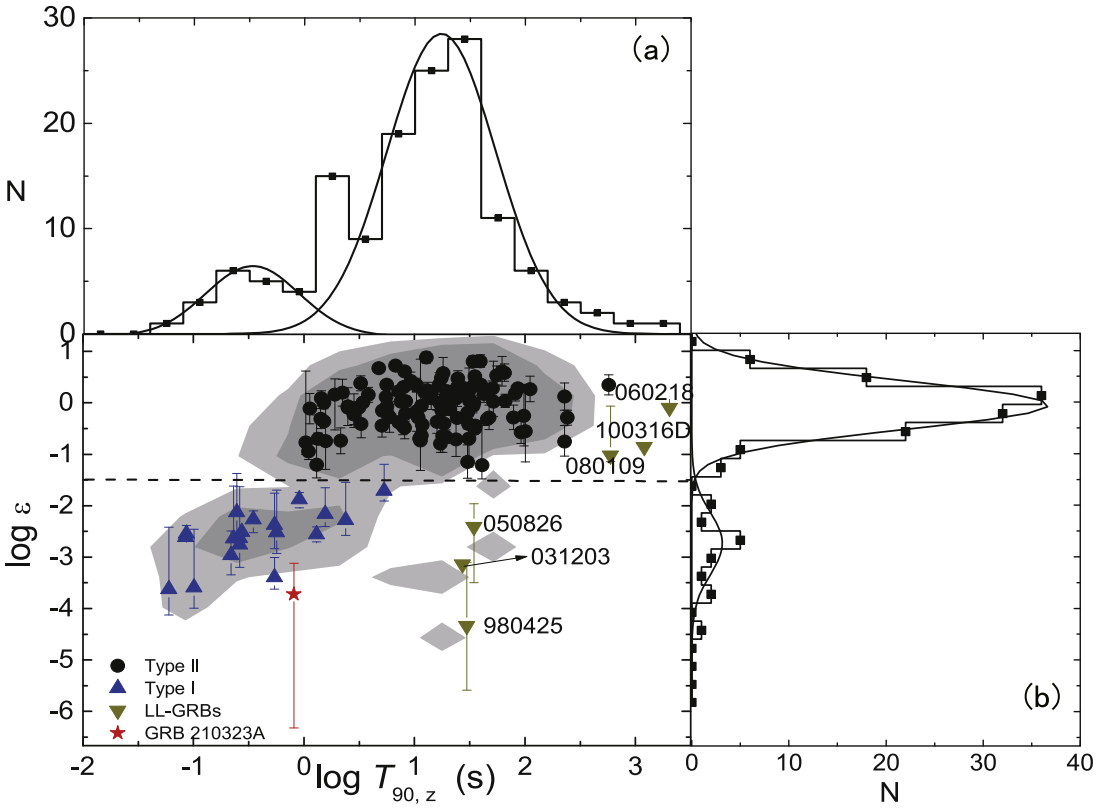

Figure 5. GRB 210323A (red star) in the log $T_{90,z}$ vs. log ε plane. 1D and 2D distributions for the GRB samples from Lü et al. (2010) in the log $T_{90,z}$ vs. log ε plane along with the bimodal fits (solid lines in panels (a) and (b)) are also shown.

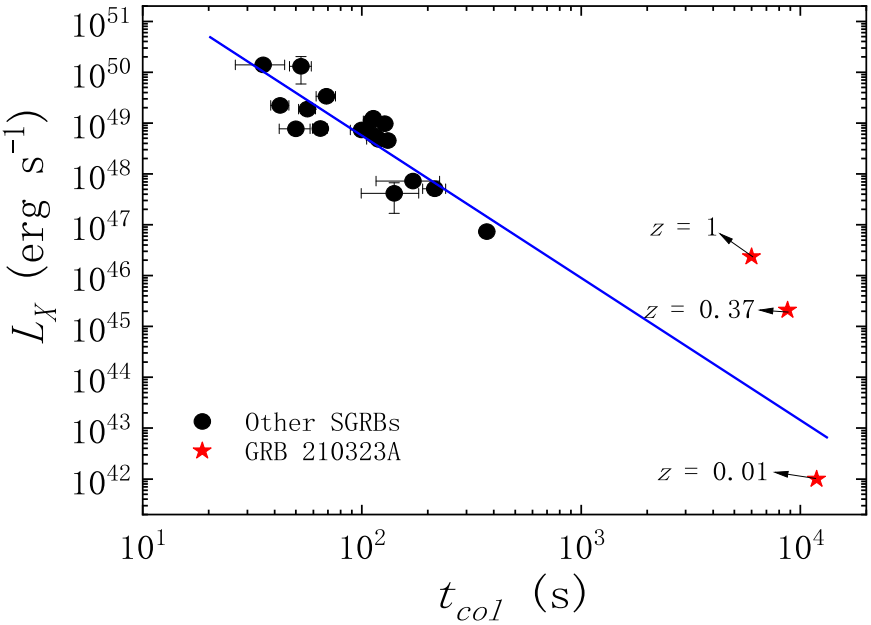

Figure 6. The collapse timescale $t_{\rm col}$ vs. X-ray luminosity $L_{\rm X}$ for GRB 210323A (red stars) with different redshift and other GRBs (black dots), along with the fit line (blue solid line) of $t_{\rm col} - L_X$.

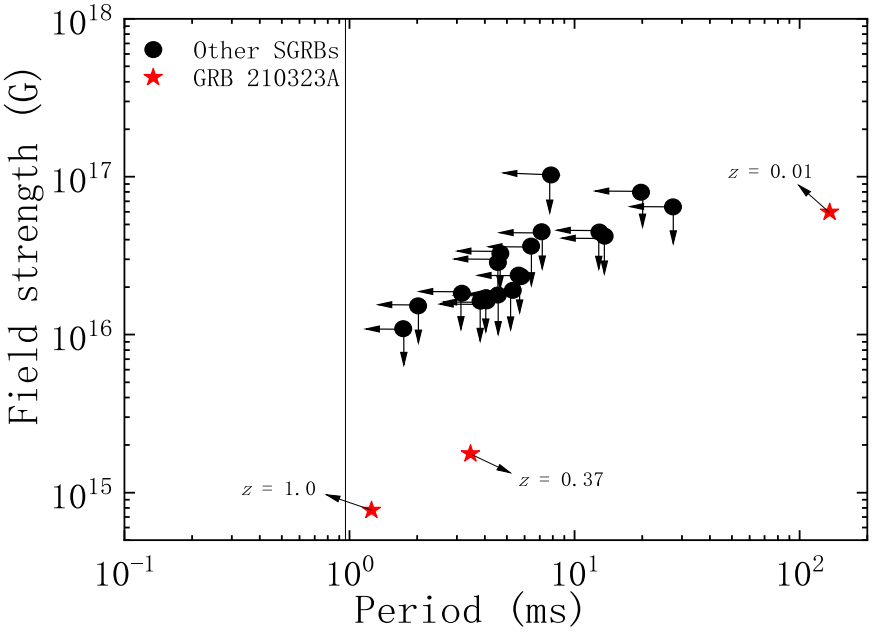

Figure 7. Inferred magnetar parameters, P_0 vs. B_p derived for GRB 210323A with different redshift (red stars). The vertical solid line is the break-up spin period limit for a neutron star (Lattimer & Prakash 2004).

By combining Equations (7) and (8), the derived parameters of magnetar B_p and P_0 can be expressed as:

$$B_{p,15} = 2.05(I_{45}R_6^{-3}L_{X,49}^{-1/2}\tau_3^{-1}), \quad (11)$$

$$P_{0,-3} = 1.42(I_{45}^{1/2}L_{X,49}^{-1/2}\tau_3^{-1/2}). \quad (12)$$

We adopt typical parameters' values of $M = 1.4M_\odot$, $R = 10^6$ cm, and $I \simeq \frac{2}{5}MR^2$. One can derive the upper limits of P_0 and B_p by using the lower limit of τ. So, the derived upper limits of B_p and P_0 can be summarized as follows, e.g., $B_p < 5.97 \times 10^{16}$ G and $P_0 < 136.16$ ms for $z = 0.01$, $B_p < 1.76 \times 10^{15}$ G and $P_0 < 3.45$ ms for $z = 0.37$, and $B_p < 7.72 \times 10^{14}$ G and $P_0 < 1.25$ ms for $z = 1$, respectively. Figure 7 presents the B_p–P_0 diagram of GRB 210323A, and comparing it with other short GRBs are also plotted in this Figure. The derived upper limit of B_p for GRB B_p seems to be less than that of other SGRBs.

4.2. Detectability of GW Radiation from Supra-massive Magnetar

If the supra-massive magnetar is indeed operating in short GRB 210323A, a possible GW radiation may be produced by the supra-massive magnetar. If the release of rotational energy is dominated by GW radiation with the frequency f_{GW}, the GW strain can be written as (Lasky & Glampedakis 2016)

$$H(t) = \frac{4GI\epsilon}{D_L c^4}\Omega(t)^2. \quad (13)$$

One has the Fourier transform of $H(t)$, $\tilde{H}(f_{GW}) = H(t)\sqrt{dt/df_{GW}}$, and the instrument noise $S(f_{GW})$ is under a stationary phase approximation. So, $\tilde{H}(f_{GW})$ can be express as

$$\tilde{H}(f_{GW}) = \frac{1}{D_L}\sqrt{\frac{5GI}{2c^3 f_{GW}}} \approx 2.6 \times 10^{-25}\left(\frac{I}{10^{-25}\ \mathrm{g\ cm^2}}\frac{1\ \mathrm{kHz}}{f_{GW}}\right)^{1/2}\left(\frac{D_L}{100\ \mathrm{Mpc}}\right)^{-1} \quad (14)$$

It is found that $\tilde{H}(f)$ does not depend on the ellipticity of the NS, but strongly depends on the angular frequency. One can estimate the characteristic amplitude of GW, (Corsi & Mészáros 2009; Lasky & Glampedakis 2016; Lü et al. 2017),

$$H_c = f_{GW}H(t)\sqrt{\frac{dt}{df_{GW}}} = \frac{f_{GW}}{D_L}\sqrt{\frac{5GI}{2c^3 f_{GW}}} \approx 8.22 \times 10^{-24}\left(\frac{I}{10^{45}\ \mathrm{g\ cm^2}}\frac{f_{GW}}{1\ \mathrm{kHz}}\right)^{1/2}\left(\frac{D_L}{100\ \mathrm{Mpc}}\right)^{-1}.$$

For GRB 210323A, the pseudo-redshift $z = 0.01$, 0.37 and 1 are adopted to do the calculations and correspond to $D_L \sim 43$ Mpc, 1981 Mpc and 6608 Mpc, respectively. By adopting the GW frequency range $f_{GW} = [120–1000]$ Hz, the maximum value of H_c can be estimated. For $z = 0.01$, 0.37 and 1, the maximum value of H_c can be estimated to be less than 6.2×10^{-22}, 1.4×10^{-23} and 4.1×10^{-24}, respectively. The GW strain sensitivity for Advanced LIGO and the Einstein Telescope (ET) are plotted in Figure 8. The GW strain of GRB 210323A is below the initial LIGO or Advanced-LIGO noise curve, and the

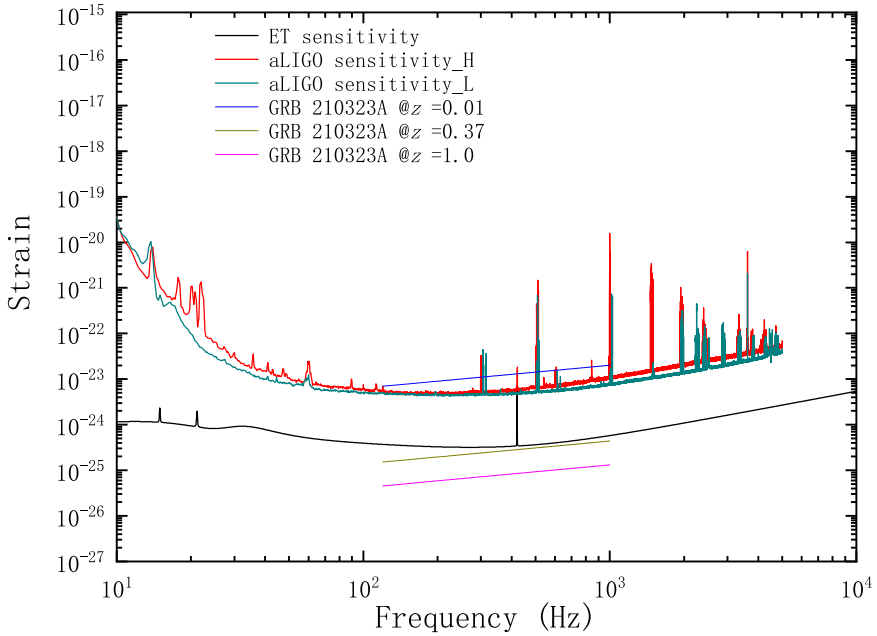

Figure 8. GW strain evolution with frequency for GRB 210323A at distances $D_{\rm L} = 43$, 1981 and 6608 Mpc (the blue, goldenrod and purple straight lines, respectively). The data of the noise curve are taken from the website: https://git.ligo.org/lscsoft/bilby/-/tree/master/bilby/gw/detector/noise_curves.

signal of GW cannot be detected, except the redshift is as low as 0.01 (less than ∼40 Mpc). However, ET may detect such a signal in the future when the redshift is less than 0.37.

4.3. Possible Kilonova Emission

NS–NS binary merger can power neutron-rich ejecta. Heavy elements with radioactivity are synthesized via *r*-process during the merger (Metzger 2017 for review), and it is believed to be the major way of producing most super-iron elements in the universe. Li & Paczyński (1998) discussed the prominent optical transients (e.g., kilonova) following mergers and offered a simple model to estimate the peak luminosity and timescales for these transients. This model only considers power injection from radioactive decay. A dynamic model for merger ejecta powered by a merger-induced millisecond-magnetar is proposed by Yu et al. (2013), and predicts a brighter optical transient.

If the central engine of short GRB 210323A is a long-lasting supra-massive NS, then, additional energy from magnetar should be contributed to kilonova emission (Yu et al. 2013; Zhang 2013; Metzger & Piro 2014; Gao et al. 2017; Yuan et al. 2021). One test is to calculate how bright of kilonova emission is by adopting the opacity $\kappa = 0.97\,{\rm cm^{-2}\,g^{-1}}$, the ejecta mass $M_{\rm ej} = 10^{-2}\,M_{\odot}$, $n = 0.01\,{\rm cm^{-3}}$ due to the mergering environment, and ejecta velocity $\beta_{ej} = 0.1c$. The light curve of AT2017gfo is fitted to obtain the above parameters (Yu et al. 2018; Hajela et al. 2019). The luminosity and energy injection timescale are roughly estimated as the plateau luminosity and collapse time in the X-ray emission.

Figure 9 presents the possible kilonova emission in *r*-band at redshift $z = 0.01$, 0.37 and 1. We also collect the upper limits of optical observations from GCN followed GRB 210323A to compare with the calculated kilonova emission (e.g., Global MASTER-Net, *S*wift/UVOT, GMOS, GTC, NOT, Mondy, Kitab and Nanshan; (Breeveld 2021; de Ugarte Postigo et al. 2021; Fu et al. 2021; Lipunov et al. 2021; Malesani et al. 2021; Pankov et al. 2021; Pozanenko et al. 2021; Rastinejad et al. 2021; Tiurina et al. 2021), and plot in Figure 9. The numerical calculation shows that the kilonova cannot be detected at redshift $z > 0.37$. However, it can be detected by several instruments (e.g., MASTER-Tavrida, NOT, GTC, and GMOS) when the redshift is as low as 0.01.

5. Conclusions

GRB 210323A is a short-duration GRB with a $T_{90} \sim 1$ s. There is no evidence of extended emission that is detected in γ-ray emission up to 30 after trigger. By extracting the time-average spectrum of prompt emission, its spectral peak energy is as high as 1826 ± 747 keV. More interestingly, it has an extremely long-lasting X-ray plateau emission with a duration of $\sim 10^4$ s, and then follows a rapid decay with a decay slope ∼3.2. No short GRBs observed before have shown the X-ray plateau emission with a duration longer $\sim 10^3$. This temporal feature can hardly be explained by invoking the afterglow model for a BH central engine. However, such a feature can be explained very well by a survived supra-massive NS as the central engine with a lifetime of hundreds of seconds.

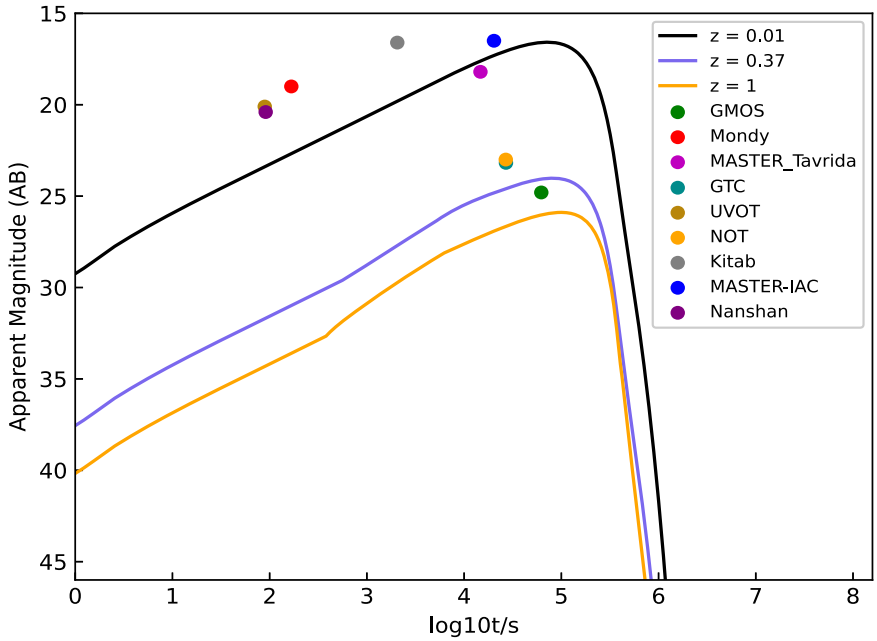

Figure 9. Kilonova emission of GRB 210323A by considering the contributions of both $r-$ process and magnetar-powered in the $r-$ band at $z = 0.01$, 0.37 and 1.0. The optical detection upper limit of various instruments for GRB 210323A is plotted as dots.

Since GRB 210323A lacks redshift information, we set a series of pseudo-redshifts from 0.01 to 1, which is a reasonable redshift range for SGRBs. By calculating the ε value and plotting the position of GRB 210323A in the $E_{\rm p}$–$E_{\gamma,\rm iso}$ diagram, it is found that short GRB 210323A seems to be following with Type I GRBs population, and they also support the origin from a merger of binary compact stars.

By assuming that the central engine of GRB 210323A is supra-massive NS, together with the feature of X-ray plateau, one can calculate the upper limits of $B_{\rm p}$ and P_0, e.g., $B_{\rm p} < 5.97 \times 10^{16}$ G and $P_0 < 136.16$ ms for $z = 0.01; B_{\rm p} < 1.76 \times 10^{15}$ G and $P_0 < 3.45$ ms for $z = 0.37; B_{\rm p} < 7.72 \times 10^{14}$ G and $P_0 < 1.25$ ms for $z = 1$. When we compare it with other short GRBs, it is found that $B_{\rm p}$ of GRB 210323A is lower by about an order of magnitude because of the low plateau luminosity (L_X). This may be natural to explain the long-surviving time of the supra-massive magnetar.

Moreover, we also estimate the upper limit for the possible GW radiation and kilonova emission. We find that the possible GW strain of supra-massive NS is less than that of the noise curve of Advanced-LIGO, and it cannot be detected, except the redshift is as low as 0.01. By taking numerical calculations, it is found that the possible kilonova cannot be detected at redshift $z > 0.37$. However, it can be detected by several instruments (e.g., MASTER-Tavrida, NOT, GTC, and GMOS) when the redshift is as low as 0.01.

In any case, the long-lasting plateau emission following a rapid decay in X-ray afterglow of GRB 210323A is an interesting case. If supra-massive magnetar is indeed operating in short GRB 210323A, together with the value of $\varepsilon-$ method and its position in the $E_{{\rm p},z}$–$E_{\gamma,\rm iso}$ diagram, one can summarize the possible origin of GRB 210323A. The progenitor of GRB 210323A is a coalescence of NS–NS, a supra-massive NS could be formed as the central engine after the NS–NS merger due to energy loss by GW radiation. The observed long-lasting X-ray plateau emission is caused by supra-massive magnetar spin-down. The subsequent abrupt decay segment can be explained by the collapsing of the supra-massive magnetar which leaves a black hole. The r-process from ejecta and additional rotation energy from magnetar can produce a kilonova. Unfortunately, the possible GW radiation and kilonova emission associated with GRB 210323A is too weak to be detected.

Acknowledgments

We acknowledge the use of public data from Fermi, Swift, and the UK Swift Science Data Centre. This work is supported by the Guangxi Science Foundation (grant No. 2023GXNSFDA026007), and the Program of Bagui Scholars Program (LHJ).

References

Abbott, B. P., Abbott, R., Abbott, T. D., et al. 2017, ApJL, 848, L13
Abbott, B. P., Abbott, R., Abbott, T. D., et al. 2017, ApJL, 851, L16
Ahumada, T., Singer, L. P., Anand, S., et al. 2021, NatAs, 5, 917
Amati, L., Frontera, F., Tavani, M., et al. 2002, A&A, 390, 81
Barthelmy, S. D., Cummings, J. R., Krimm, H. A., et al. 2021, GCN, Circular Service, No. 29721, 1
Beardmore, A. P., Evans, P. A., Ambrosi, E., et al. 2021, GCN, Circular Service, No. 29705, 1

Berger, E., Fong, W., & Chornock, R. 2013, ApJL, 774, L23
Breeveld, A. A., Gropp, J. D. & Swift/UVOT Team 2021, GCN, Circular Service, No. 29712, 1
Chang, X.-Z., Lü, H.-J., Yang, X., et al. 2023, ApJ, 943, 146
Chen, W., Xie, W., Lei, W.-H., et al. 2017, ApJ, 849, 119
Corsi, A., & Mészáros, P. 2009, ApJ, 702, 1171
Dai, Z. G., & Lu, T. 1998, A&A, 333, L87
Dai, Z. G., & Lu, T. 1998, PhRvL, 81, 4301
de Ugarte Postigo, A., Kann, D. A., Malesani, D. B., et al. 2021, GCN, Circular Service, No. 29717, 1
Du, Z., Lü, H., Yuan, Y., et al. 2024a, ApJL, 962, L27
Du, Z.-W., Lü, H., Liu, X., et al. 2024b, MNRAS, 529, L67
Ferro, M., Brivio, R., D'Avanzo, P., et al. 2023, A&A, 678, A142
Fu, S. Y., Zhu, Z. P., Liu, X., et al. 2021, GNC, Circular Service, No. 29700, 1
Gao, H., Zhang, B., & Lü, H.-J. 2016, PhRvD, 93, 044065
Gao, H., Zhang, B., Lü, H.-J., et al. 2017, ApJ, 837, 50
Gehrels, N., Norris, J. P., Barthelmy, S. D., et al. 2006, Natur, 444, 1044
Goldstein, A., Veres, P., Burns, E., et al. 2017, ApJL, 848, L14
Gropp, J. D., Marshall, F. E., Moss, M. J., et al. 2021, GNC, Circular Service, No. 29699, 1
Hajela, A., Margutti, R., Alexander, K. D., et al. 2019, ApJL, 886, L17
Hamburg, R., Meegan, C. & Fermi GBM Team 2021, GNC, Circular Service, No. 29709, 1
Jin, Z.-P., Hotokezaka, K., Li, X., et al. 2016, NatCo, 7, 12898
Kouveliotou, C., Meegan, C. A., Fishman, G. J., et al. 1993, ApJL, 413, L101
Kumar, P., & Zhang, B. 2015, PhR, 561, 1
Lan, L., Lü, H.-J., Zhong, S.-Q., et al. 2018, ApJ, 862, 155
Lasky, P. D., & Glampedakis, K. 2016, MNRAS, 458, 1660
Lattimer, J. M., & Prakash, M. 2004, Sci, 304, 536
Lei, W. H., Wang, D. X., Zhang, L., et al. 2009, ApJ, 700, 1970
Levan, A. J., Tanvir, N. R., Ackley, K., et al. 2023, jwst.prop, 1, 4445
Li, L.-X., & Paczyński, B. 1998, ApJL, 507, L59
Liang, E., Zhang, B., Virgili, F., et al. 2007, ApJ, 662, 1111
Lipunov, V., Gorbovskoy, E., Kornilov, V., et al. 2021, GNC, Circular Service, No. 29702, 1
Liu, T., Gu, W.-M., & Zhang, B. 2017, NewAR, 79, 1
Lü, H.-J., Liang, E.-W., Zhang, B.-B., et al. 2010, ApJ, 725, 1965
Lü, H.-J., Yuan, H.-Y., Yi, T.-F., et al. 2022, ApJL, 931, L23
Lü, H.-J., Zhang, B., Lei, W.-H., et al. 2015, ApJ, 805, 89
Lü, H.-J., Zhang, H.-M., Zhong, S.-Q., et al. 2017, ApJ, 835, 181
Malesani, D. B., de Ugarte Postigo, A., Zhu, Z., et al. 2021, GNC, Circular Service, No. 29703, 1
Metzger, B., Martínez-Pinedo, G., Darbha, S., et al. 2010, MNRAS, 406, 2650
Metzger, B. D. 2017, LRR, 20, 3
Metzger, B. D., Giannios, D., Thompson, T. A., et al. 2011, MNRAS, 413, 2031
Metzger, B. D., & Piro, A. L. 2014, MNRAS, 439, 3916
Paczynski, B. 1986, ApJL, 308, L43
Paczynski, B. 1991, AcA, 41, 257
Pankov, N., Pozanenko, A., Novichonok, A., et al. 2021, GCN, Circular Service, No. 29710, 1
Popham, R., Woosley, S. E., & Fryer, C. 1999, ApJ, 518, 356
Pozanenko, A., Pankov, N., Klunko, E., et al. 2021, GCN, Circular Service, No. 29708, 1
Qin, Y., Liang, E.-W., Liang, Y.-F., et al. 2013, ApJ, 763, 15
Rastinejad, J., Paterson, K., Fong, W., et al. 2021, GCN, Circular Service, No. 29720, 1
Roming, P. W. A., Kennedy, T. E., Mason, K. O., et al. 2005, SSRv, 120, 95
Rowlinson, A., O'Brien, P. T., Tanvir, N. R., et al. 2010, MNRAS, 409, 531
Sun, H., Wang, C.-W., Yang, J., et al. 2023, arXiv:2307.05689
Tiurina, N., Lipunov, V., Kornilov, V., et al. 2021, GCN, Circular Service, No. 29724, 1
Troja, E. 2023, Univ, 9, 245
Troja, E., Cusumano, G., O'Brien, P. T., et al. 2007, ApJ, 665, 599
Troja, E., Fryer, C. L., O'Connor, B., et al. 2022, Natur, 612, 228
Usov, V. V. 1992, Natur, 357, 472
Yang, B., Jin, Z.-P., Li, X., et al. 2015, NatCo, 6, 7323
Yang, J., Ai, S., Zhang, B.-B., et al. 2022, Natur, 612, 232
Yu, Y.-W., Liu, L.-D., & Dai, Z.-G. 2018, ApJ, 861, 114
Yu, Y.-W., Zhang, B., & Gao, H. 2013, ApJL, 776, L40
Yuan, Y., Lü, H.-J., Yuan, H.-Y., et al. 2021, ApJ, 912, 14
Zhang, B. 2006, Natur, 444, 1010
Zhang, B. 2013, ApJL, 763, L22
Zhang, B. 2018, The Physics of Gamma-Ray Bursts (Cambridge: Cambridge Univ. Press)
Zhang, B., & Mészáros, P. 2001, ApJL, 552, L35
Zhang, B., Zhang, B.-B., Virgili, F. J., et al. 2009, ApJ, 703, 1696
Zhang, B.-B., Liu, Z.-K., Peng, Z.-K., et al. 2021, NatAs, 5, 911
Zhang, B.-B., Uhm, Z. L., Connaughton, V., et al. 2016, ApJ, 816, 72
Zhang, B.-B., Zhang, B., Sun, H., et al. 2018, NatCo, 9, 447
Zhong, S.-Q., Li, L., Xiao, D., et al. 2024, ApJL, 963, L26